Chemical Engineering Journal 166 (2011) 607–615

Contents lists available at ScienceDirect

Chemical Engineering Journal

journal homepage: www.elsevier.com/locate/cej

Modeling the transient cyclic operation of a commercial NSR catalyst

J.S. Mandur, M. Al-Harbi, W.S. Epling, H.M. Budman *

Department of Chemical Engineering, University of Waterloo, 200 University Av, Waterloo, ON, Canada N2L3G1

ARTICLE INFO

Article history:
Received 17 August 2010
Received in revised form 7 November 2010
Accepted 8 November 2010

Keywords:
NO_x storage
NO_x reduction
Steady cyclic operation
Transient cyclic operation
Mathematical model

ABSTRACT

A pseudo 1-D model of an industrial NO_x storage and reduction (NSR) catalyst has been developed under isothermal conditions. The Pt/Ba proximity or the presence of barium in different chemical forms such as BaO and $BaCO_3$ can result in a wide range of storage rates. To represent these multiple storage sites, an idealized storage particle with a spherical configuration is proposed where the outer layer is assumed to represent the sites with the highest storage capacities/rates while subsequently deeper layers represent the sites with relatively lower storage capacities. It is further assumed that the NO_x species first react with the particles in the outer layer, followed by the particles in subsequent deeper layers. To model the progressively decreasing storage rates, a shrinking core approach is used with a diffusivity coefficient, decreasing nonlinearly along the particle depth. The degree of nonlinearity depends on the complexity of the catalyst and therefore, depending on the catalyst, being studied, one can calibrate this function instead of quantifying different types of storage sites.

During cyclic operation starting with a completely regenerated catalyst, model predictions for the NO_x concentration profiles are in a good agreement with the experimental data during both the transient and steady cycle-to-cycle regimes. It is also shown that with limited amount of reductant, the regeneration of storage sites takes place only in the front portion of the catalyst up to a certain length and the remaining part of the catalyst is only involved in the storage reactions. After a certain number of cycles, the back of the catalyst reaches its saturation limit for storing NO_x and from then on, only the amount of catalyst being regenerated in the front part of the catalyst during the rich phase participates in storage.

1. Introduction

Although lean-burn engines are more fuel efficient than standard stoichiometric-burn engines, the conventional after-treatment systems based on three way catalysis are not effective in reducing the nitrogen oxides (NO_x) from an oxygen-rich exhaust. One of the recent developments in after-treatment systems for such exhaust conditions is the NO_x storage and reduction (NSR) catalyst. This catalyst contains alkali or alkaline earth metal compounds which store the NO_x in the form of nitrates/nitrites when exposed to oxygen-rich exhaust. When the catalyst reaches a certain level of saturation in terms of NO_x storage, an excess of fuel is injected into the engine or exhaust pipe resulting in a reductant-rich exhaust. In this reducing environment, the previously stored NO_x is released from the storage particles and subsequently reduced to N_2. The overall cycle can be divided into two phases: a lean phase corresponding to normal engine operation and a rich phase corresponding to fuel-rich injection.

There are a number of catalytic reactions involved in the process and over the past few years, several approaches have been proposed to model these reactions, thus enabling better understanding of storage and reduction dynamics [1–9]. Fig. 1 shows a simulated NO_x concentration profile obtained when a completely regenerated catalyst is exposed to oxygen-rich exhaust for a long period. As shown, rapid NO_x storage occurs during the initial period, followed by a slow increase in effluent NO_x. This behavior has been attributed to mass transport limitations in the NO_x storage process [10–12]. However, it is uncertain whether these mass transfer limitations are present in the wash-coat or within the barium particles or both. The proposed global kinetic model by Olsson et al. [1,2] accounted for these mass transfer limitations within the storage particles using a shrinking core concept. In this approach, a spherical structure of barium carbonate was assumed and as storage proceeds, the outer surface of carbonate sphere reacted first, forming a nitrate layer of uniform thickness. Therefore, for further storage, the NO_x species have to diffuse through the nitrate layer, which keeps growing in thickness as the storage proceeds. A similar diffusion approach within the storage particles was used by Tuttlies et al. [7] with an additional hypothesis that the diffusion is strongly affected by a change in solid volume when barium carbonate gets converted into barium nitrate. In a recent study by Kromer et al. [8],

* Corresponding author. Tel.: +1 519 888 4567x36980.
E-mail addresses: hbudman@cape.uwaterloo.ca, hbudman@uwaterloo.ca (H.M. Budman).

1385-8947/$ – see front matter © 2010 Elsevier B.V. All rights reserved.
doi:10.1016/j.cej.2010.11.032

Nomenclature

v	linear gas velocity (m/s)
a	mass transfer surface area per unit channel volume (m^{-1})
k_c	mass transfer coefficient (m/s)
C_{gi}	bulk phase concentration of ith gas species (mol/m^3)
C_{si}	washcoat phase concentration of ith gas species (mol/m^3)
C_{fi}	concentration of ith gas species at the interface within the catalyst (mol/m^3)
R_d	rate of diffusion through the nitrate layer within the NO_x storage particle
θ_m	fraction of mth catalytic site
R_j^f	rate of jth reaction occurring at the interface within the catalyst (mol/m^3)
R_j^s	rate of jth reaction occurring at the catalyst surface (mol/m^3)
$v_{i,j}$	stoichiometric coefficient for ith gas species undergoing jth reaction
$v_{m,j}$	stoichiometric coefficient for mth catalytic site consumed in jth reaction
ψ_m^{cap}	storage capacity of mth catalytic site per washcoat volume (mol/m^3)
t	time (s)
z	axial coordinate (m)
ε^s	porosity of washcoat
ε^g	ratio of bulk to total channel volume
I	number of gas species
J	number of reactions
M	number of catalytic sites
r	radial coordinate within the proposed NO_x storage particle (m)
r_f	radial position of the interface within the proposed NO_x storage particle (m)
r_{tot}	total radius of the proposed storage particle (m)
D	diffusivity coefficient within the storage particle (m^2/s)
D_{eff}	effective diffusivity coefficient within the storage particle (m^2/s)

two different one-dimensional NO_x storage models were proposed to account for these mass transfer limitations. In one model, two layers of particles were considered and it was proposed that once the NO_x is stored on the particles in the first layer, it diffuses to the second layer for further reaction. Therefore, the overall storage step is controlled by the mass transfer coefficient between these two layers. In the second model, two parallel pathways with relatively different rates were suggested to account for the effect of neighboring Pt and Ba particles on NO_x storage. The presence of multiple types of washcoat layers with different properties, especially in complex catalyst formulations, can also result in different storage rates. In one of their studies, Kočí et al. [3] considered a differentiated catalyst with two washcoat layers where, one layer has storage components active at lower temperature and another layer has storage components active at higher temperature.

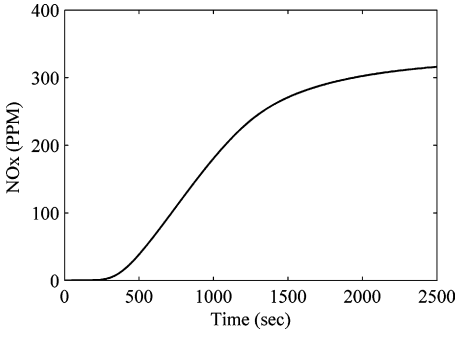

Fig. 1. Simulated NO_x concentration profile at the catalyst exit during a long lean phase.

Although these models have been able to explain the experimental data used for their formulation and validation, their applicability to different catalyst formulations and different gas concentrations is questionable. For example, for some catalyst formulations, if the number of different storage sites is more than what has been assumed in the above models, due to either the occurrence of different storage species or varying Pt/Ba proximity, the results may be unsatisfactory. Accordingly, one of the key motivations behind this paper is to propose a mathematical approach which can describe the storage dynamics without quantifying the different types of storage particles and therefore, can be applicable to any catalyst formulation.

When engine operation is alternating between lean and rich phase feed conditions, a typical cyclic NO_x concentration profile, similar to the one shown in Fig. 2, is observed. If the net amount of reductants entering the catalyst during the rich phase is insufficient to regenerate the storage sites completely, the overall storage capacity of the catalyst will keep decreasing in subsequent cycles until equilibrium between the number of storage sites used during the lean phase and then regenerated during the next rich phase is achieved. Until such equilibrium is reached, an initial transient period is observed that will be referred to hereafter as the "transient cyclic regime", whereas the later period, during which cycle-to-cycle equilibrium is maintained, will be referred to as the "steady cyclic regime". In real life operation, it is expected that the varying driving conditions due to engine start-up operation, sudden acceleration, non-uniform braking and varying road conditions will result in more complex operation with a mix of transient and steady cyclic regimes. As a result, the exhaust system is expected to operate in the transient cyclic regimes most of the time. For example, Fig. 2 shows a NO_x concentration profile at the reactor exit during the startup of cyclic operation. As shown, the system is under the transient cyclic regime for nearly an hour until steady cyclic conditions are reached, which is a really long period of operation when considering average city driving. Therefore, prediction and optimization of an NSR catalyst requires a model that can describe both the transient and steady cyclic regimes. Although an incomplete regeneration is one of the key factors governing the dynamics during transient cyclic regime, it is also very important to understand how the regeneration process proceeds within the particle and also along the catalyst length. Tuttlies et al. [7] reported different time scales between storage and reduction dynamics and were able to explain this difference by considering the fact that barium carbonate has lower molar volume than barium nitrate. During the storage process, barium carbonate gets converted into barium nitrate and therefore the particle becomes denser as storage proceeds. However, during the regeneration phase, the formation of barium carbonate results in opening of the pores and as a result, the reductants can more easily penetrate the whole particle which results in very high regeneration rates. In addition to the comparison between experimental and simulated % NO_x conversion over different cycles in the transient cyclic regime, the authors also presented insight regarding the position of carbonate–nitrate interface within the particle. This concept was further expanded by Schmeißer et al. [6], where the authors compared experimental and simulated NO_x concentration profiles over two consecutive cycles in the transient cyclic regime.

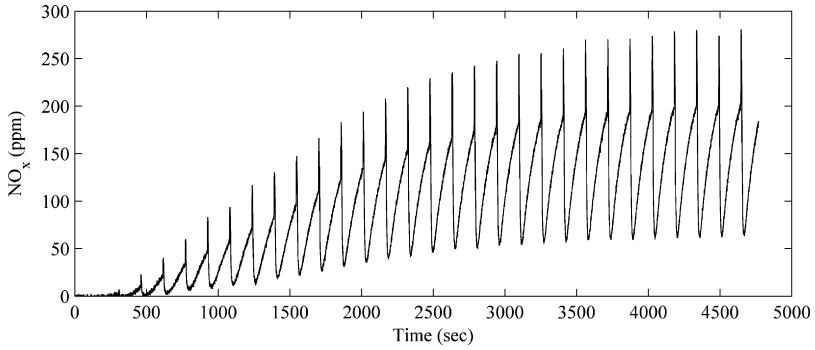

Fig. 2. Measured NO_x concentration profile at the catalyst exit during a cyclic operation, starting with completely regenerated catalyst. Lean phase composition: 330 ppm NO, 10% O_2, 5% CO_2, 5% H_2O and rest N_2. Rich phase composition: 1.5% CO, 5% CO_2, 5% H_2O and rest N_2.

In this work, a pseudo 1-D model of a commercial NSR catalyst is presented. To represent the multiple NO_x storage sites with different capacities, an idealized catalyst storage particle is proposed in which the outer layer is assumed to represent the sites with the highest storage capacities while subsequently deeper layers represent the sites with relatively lower storage capacities. The decreasing storage capacity, along the particle depth, is considered as equivalent to increasing mass transfer resistance to the storage particle as NO_x penetrates the particle. Mathematically, a shrinking core model, adapted from Olsson et al. [1], is used with a diffusivity coefficient, which decreases nonlinearly along the particle depth, thus representing the increasing mass transfer resistance. The proposed diffusivity function can be calibrated according to the catalyst being studied and therefore, eliminates the need to quantify different types of storage sites. In the second part, the paper provides insights regarding the regeneration process over different cycles for the start-up cyclic operation.

2. Modeling

The Pt/Ba-based catalyst used in this study was supplied by Johnson Matthey. The test sample was cut into a cylindrical shape from a larger monolith block having a cell density of 300 cells per square inch. The resulting sample was 3 in. long and 0.91 in. in diameter with a total of 169 channels. Details about the experimental setup used to collect the data are described in Al-Harbi and Epling [13].

The channel space can be divided into two phases: a bulk phase, representing an open area for the flow of gas and a washcoat phase in which the gas species first diffuse from the bulk and then undergo a series of catalytic reactions. The gaseous reaction products from the washcoat phase then diffuse back into the bulk and exit the system with the rest of the gas stream. In order to simplify the model, the following major assumptions were made:

1. Due to the large L/D ratio of the bulk phase (∼60), radial gradients in the bulk gas concentration are neglected. Since the washcoat thickness is even smaller than the bulk diameter (by a factor of ∼30), the radial gradients within the washcoat phase gas concentrations are also neglected. Instead, the effect of concentration boundary layers across the bulk and washcoat phases is accounted for using a lumped mass transfer coefficient between the phases.
2. Under similar operating conditions, as used for this study, Al-Harbi et al. [14] observed a rise in the temperature only during the rich phase which then diminishes gradually during the subsequent lean phase and at 400 °C, the maximum temperature rise in the catalyst was reported to be 15–30 K. In the cyclic experiments conducted at 300 °C, in this study, the temperature profiles are observed to follow the similar cyclic pattern with the maximum rise of only 18 K, recorded at the catalyst exit. In the later section on results and discussion, it is shown that when the kinetic parameters, estimated from the data obtained under Mixture 2 (cf. Table 2), were used to predict the data obtained under Mixture 3 (cf. Table 2), the average difference in the experimental and the simulated exit NO_x concentration is observed to be only about 3% of the input NO_x. With this observation, it seems reasonable to neglect the effect of temperature rise for this study

Table 1
List of the reactions with their corresponding rate expressions.

Reaction	Rate expressions
$NO + \frac{1}{2}O_2 \overset{r_1}{\longleftrightarrow} NO_2$	$r_1 = k_1 * (C_{NO} * c_{O_2}^{0.5} - (c_{NO_2}/K_1^{eq}))/(1 + K_1 * c_{NO_2}^{0.7})$
$2NO_2 + \frac{1}{2}O_2 + BaCO_3 \overset{r_2}{\longrightarrow} Ba(NO_3)_2 + CO_2$	$r_2 = \psi_{NO_x} * \frac{k_2}{1+k_2*((r_{tot}-r_f)/D_{eff_{NO_2}})*(r_f/r_{tot})*\theta_{BaCO_3}} * C_{NO_2} * \theta_{BaCO_3} * c_{O_2}^{0.25}$
$2NO + \frac{3}{2}O_2 + BaCO_3 \overset{r_3}{\longrightarrow} Ba(NO_3)_2 + CO_2$	$r_3 = \psi_{NO_x} * \frac{k_3}{1+k_3*((r_{tot}-r_f)/D_{eff_{NO}})*(r_f/r_{tot})*\theta_{BaCO_3}} * C_{NO} * \theta_{BaCO_3} * c_{O_2}^{0.75}$
$Ba(NO_3)_2 + CO_2 \overset{r_4}{\longrightarrow} NO + \frac{3}{2}O_2 + BaCO_3$	$r_4 = k_4 * \psi_{NO_x} * \frac{1}{(1+\exp(-X_1*(\theta_{Ba(NO_3)_2}-Y_1)))}$
$Ba(NO_3)_2 + CO_2 \overset{r_5}{\longrightarrow} 2NO_2 + \frac{1}{2}O_2 + BaCO_3$	$r_5 = k_5 * \psi_{NO_x} * \frac{1}{(1+\exp(-X_2*(\theta_{Ba(NO_3)_2}-Y_2)))}$
$Ce_2O_3 + \frac{1}{2}O_2 \overset{r_6}{\longrightarrow} CeO_2$	$r_6 = k_6 * \psi_{O_2} * C_{O_2} * (1 - \theta_{CeO_2})$
$CO + 2CeO_2 \overset{r_7}{\longrightarrow} CO_2 + Ce_2O_3$	$r_7 = \psi_{O_2} * \frac{k_7}{1+K_7*((r_{tot}-r_f)/D_{eff_{CO\_Ce}})*(r_f/r_{tot})*\theta_{CeO_2}} C_{CO} * \theta_{CeCO_2}$
$CO + \frac{1}{2}O_2 \overset{r_8}{\longrightarrow} CO_2$	$r_8 = k_8 * \psi_{NO_x} * \frac{C_{CO}*C_{O_2}}{(1+K_8*C_{CO})^2*(1+K_1*c_{NO_2}^{0.7})}$
$3CO + Ba(NO_3)_2 \overset{r_9}{\longrightarrow} BaCO_3 + 2NO + 2CO_2$	$r_9 = \psi_{NO_x} * \frac{k_9}{1+k_9*((r_{tot}-r_f)/D_{eff_{CO}})*(r_f/r_{tot})*\theta^2_{Ba(NO_3)_2}} * C_{CO} * \theta^2_{Ba(NO_3)_2}$
$5CO + Ba(NO_3)_2 \overset{r_{10}}{\longrightarrow} BaCO_3 + N_2 + 4CO_2$	$r_{10} = \psi_{NO_x} * \frac{k_{10}}{1+k_{10}*((r_{tot}-r_f)/D_{eff_{CO}})*(r_f/r_{tot})*\theta^2_{Ba(NO_3)_2}} * C_{CO} * \theta^2_{Ba(NO_3)_2}$
$CO + NO \overset{r_{11}}{\longrightarrow} CO_2 + \frac{1}{2}N_2$	$r_{11} = k_{11} * C_{CO} * C_{NO}$

and therefore, isothermal conditions were assumed throughout the reactor.
3. For the 1.5 m/s gas velocity used in this study, the resulting residence time in the channel is almost negligible (about 0.05 s). Correspondingly, the rate of axial convection was assumed very high compared to the rate of axial dispersion and, therefore, the latter was neglected.
4. All the reactions were assumed to be catalytic and therefore, variations in the concentration of gas species due to chemical reactions were assumed to occur only within the washcoat phase.
5. Although the storage sites can be present in different chemical forms, such as BaO and $BaCO_3$, the proposed storage particle was assumed to be $BaCO_3$. Therefore, the storage process can be represented by a relatively small number of reactions, thus lowering the number of kinetic parameters to be estimated. However, the effect of different storage sites on the overall storage capacity is accounted for using a varying diffusivity coefficient in the proposed shrinking core model. Similarly, barium nitrate was assumed to represent any possible mixture of nitrates and nitrites.
6. A certain amount of CO may get converted into H_2 through the water–gas shift reaction. Since only one temperature is considered in this work, the reaction rates corresponding to H_2 were confounded into the CO-based reaction rates. However, for different temperatures and feed compositions involving a mixture of CO and H_2, the effect of CO– and H_2–based reactions cannot be combined and would have to be considered separately, at least at low temperature.

Based on these assumptions, the change in the bulk phase concentration of the ith gas species, C_{gi}, is governed by its axial convective flow along the channel length and simultaneous diffusion into the washcoat layer (cf. Eq. (1)), while the change in the washcoat phase concentration of the ith gas species, C_{si}, is due to its diffusion from the bulk phase into the washcoat layer and subsequent consumption due to catalytic reactions (cf. Eq. (2)). The net change in the fraction of catalytic sites, θ_m, which undergoes substantial change during different catalytic reactions, is given by Eq. (3):

$$\frac{\partial C_{gi}}{\partial t} = -v\frac{\partial C_{gi}}{\partial z} + \frac{k_c a}{\varepsilon^g}(C_{si} - C_{gi}) \tag{1}$$

$$\frac{\partial C_{si}}{\partial t} = \frac{k_c a}{\varepsilon^s * (1-\varepsilon^g)}(C_{gi} - C_{si}) + \frac{1}{\varepsilon^s}\left(\sum_{j=1}^{J} v_{i,j} R_j^f\right) + \frac{1}{\varepsilon^s}\left(\sum_{j=1}^{J} v_{i,j} R_j^s\right) \tag{2}$$

$$\frac{\partial \theta_m}{\partial t} = \frac{1}{\psi_m^{cap}}\left(\sum_{j=1}^{J} v_{m,j} R_j^f\right) \tag{3}$$

where $i = 1, \ldots, I$ and $n = 1, \ldots, M$.

The initial and boundary conditions are as follows:

$$C_{gi}(z)_{t=0} = 0 \quad C_{si}(z)_{t=0} = 0 \tag{4}$$

$$C_{gi}(t)_{z=0} = C_{inlet} \tag{5}$$

$$\theta_{BaCO_3}(z)_{t=0} = 1 \quad \theta_{Ba(NO_3)_2}(z)_{t=0} = 0 \tag{6}$$

$$\theta_{Ce_2O_3}(z)_{t=0} = 1 \quad \theta_{CeO_2}(z)_{t=0} = 0 \tag{7}$$

All the considered reactions with their corresponding rate expressions are listed in Table 1. The NO oxidation reaction has been reported to be strongly inhibited by NO_2 [15] and therefore, the corresponding rate kinetics, initially based on reaction stoichiometry, were modified to include an additional NO_2 inhibition term (cf. reaction (1); Table 1). The presence of multiple types of storage sites due to either varying Pt/Ba proximity or the existence of storage particles in different chemical forms, such as BaO and $BaCO_3$ is expected to result in multiple storage reactions with different storage capacities. To account for this effect, the kinetics for NO and NO_2 storage reactions (cf. reactions (2) and (3); Table 1) were modified using a shrinking core approach. To represent the multiple types of storage sites, mathematically, an idealized equivalent storage particle was used with a spherical configuration as shown in Fig. 3. The outer layer of this particle was assumed to represent the storage sites with maximum storage capacity whereas this capacity progressively decreases as a function of depth within the particle, therefore representing the sites with decreasing storage capacities or rates in subsequent inner layers. Accordingly, starting with a fresh catalyst, the NO_x will first react with the outer layer particles forming a uniform layer of nitrates, which progressively increases in thickness as storage proceeds. The approach is similar to the one proposed by Olsson et al. [1], with a major difference being that the different layers within the proposed equivalent particle in this work represent multiple types of storage sites. To account for the decreasing storage capacity in this multilayered arrangement, a varying diffusivity coefficient was used which decreases nonlinearly as a function of particle depth, making further storage progressively more difficult as storage increases. For example, let us consider the NO_2 storage reaction. The rate at which NO_2 diffuses through the nitrate layer, R_d, can be defined according to Fick's first law of diffusion as follows:

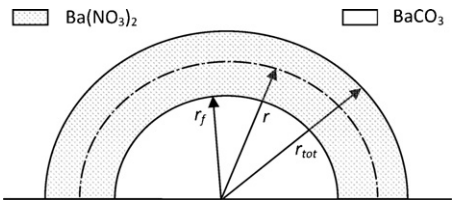

Fig. 3. Schematic representation of the storage particle in shrinking core model.

$$R_d = D(r) * (4\pi r^2) * \frac{dC_{NO_2}}{dr} \tag{8}$$

The above equation can be integrated between the surface and the interface, as follows:

$$\frac{4\pi}{R_d}\int_{C_{s_{NO_2}}}^{C_{f_{NO_2}}} dc = \int_{r_{tot}}^{r_f}\left(\frac{dr}{D(r) * r^2}\right) \tag{9}$$

To simplify the integration, the integrand on the right hand side was expressed, by defining an effective diffusivity coefficient, D_{eff}, as follows:

$$\int_{r_{tot}}^{r_f}\left(\frac{dr}{D(r) * r^2}\right) = \frac{1}{D_{eff}(r_f)}\int_{r_{tot}}^{r_f}\frac{dr}{r^2} \tag{10}$$

Integrating the modified equation, obtained after combining Eqs. (9) and (10), results in an algebraic expression similar to the one derived by Olsson et al. [1] in their shrinking core approach, as follows:

$$R_d = \frac{4\pi D_{eff}(r_f)}{(1/r_{tot}) - (1/r_f)} * (C_{f_{NO_2}} - C_{s_{NO_2}}) \tag{11}$$

Since the amount of NO_2 diffusing through the nitrate layer is assumed to react completely at the interface, the rate of diffusion can be equated to the rate of reaction at the interface. Based on

reaction stoichiometry, the reaction rate is as follows:

$$R^{f}_{NO} = k_2 C_{f_{NO_2}} C^{0.25}_{f_{O_2}} \theta_{BaCO_3} \quad (12)$$

After equating Eqs. (11) and (12), the obtained expression was rearranged to express the NO_2 concentration at the interface, $C_{f_{NO_2}}$ in terms of its concentration at the surface, $C_{s_{NO_2}}$ which when substituted into Eq. (12) results in the modified rate expression for NO_2 storage as listed in Table 1 (cf. reaction (2)). Additional details of these derivation steps can be found in the work by Olsson et al. [1]. Following similar steps, the modified rate expression for NO storage as listed in Table 1 (cf. reaction (3)) was derived. For this study, the nonlinear function for the effective diffusivity coefficient was modeled using a sigmoid as follows:

$$D_{eff}(r_f) = A * \frac{\exp(-B*(1 - r_f/r_{tot} - C))}{1 + \exp(-B*(1 - r_f/r_{tot} - C))} \quad (13)$$

Here, A, B and C are tuning parameters for the sigmoid.

The expression for the diffusivity coefficient $D(r_f)$ can be back-calculated from $D_{eff}(r_f)$ by rearranging Eq. (10) as follows:

$$D(r_f) = \frac{1}{r_f^2 * (d/dr_f)\left((1/D_{eff}(r_f))\int_{r_{tot}}^{r_f} dr/r^2\right)} \quad (14)$$

$$D(r_f) = \frac{1}{\exp(B*(1 - r_f/r_{tot} - C)) * ((1/A) + (r_f/r_{tot}) * (B/A) - (r_f^2/r_{tot}^2) * (B/A)) + (1/A)} \quad (15)$$

The NO and NO_2 storage reactions were also considered reversible in order to account for the self-decomposition of nitrates (see reactions (4) and (5); Table 1). The amount of CO_2 in the experiments for this study is very high (up to 5%) as compared to the NO_x (330 ppm) and therefore, unlike the NO_x storage reactions, it was assumed that all the nitrate particles get exposed to the CO_2 at the same time. Moreover, in the absence of any information regarding different reactivities of nitrate particles towards the self-decomposition reactions, it was further assumed that all the nitrate particles undergo the self-decomposition reaction at the same rate. Accordingly, the possibility of any mass transfer limitation in their rate expressions was eliminated for this study. From preliminary simulations, the kinetics of these backward or self-decomposition reactions were observed to be a nonlinear function of nitrate fraction and, therefore, modeled using a sigmoid function with X_1, Y_1, X_2 and Y_2 as tuning parameters (c.f. reactions (4) and (5); Table 1). The rate expression for the CO oxidation reaction (cf. reaction (8); Table 1) was adapted from the literature [17]. Since there is no propylene used in this study, the propylene inhibition term was removed from the kinetic term. The oxygen storage compounds, like ceria, have a tendency to store oxygen during the lean phase, generally represented by an oxygen storage capacity (OSC) of the catalyst. When the catalyst with partially reduced OSC after the lean phase is exposed to reductants, a certain amount of reductants gets consumed in regenerating the OSC [16]. The rate expressions for corresponding ceria oxidation and reduction reactions (cf. reactions (6) and (7), respectively; Table 1) were simply obtained on the basis of reaction stoichiometry. The relatively lower amounts of CO may not be sufficient to reach all the ceria particles at the same rate. Therefore, the ceria reduction reaction was modified according to the shrinking core approach to account for rate variability. The reductants can regenerate the storage sites using two different pathways: one releasing NO and another forming N_2 directly (cf. reactions (9) and (10), respectively; Table 1). From preliminary simulations, it was observed that for the feed compositions used to calibrate the proposed model, the regeneration reactions can be considered without mass transfer limitation. Also, the kinetics for these reactions were initially modeled based on the reaction stoichiometry, but later second order rates with respect to nitrates resulted in better fitting and the kinetics were modified accordingly. The reactions rates were further modified according to the shrinking core approach, as done with the ceria reduction reaction as discussed above. Finally, the rate expression for the reduction of released NO to N_2 was obtained based on reaction stoichiometry.

The system of partial and ordinary differential Eqs. (1)–(3) was then solved using COMSOL Multiphysics (Ver. 3.4) in combination with MATLAB (2009b).

3. Results and discussion

Two different operating scenarios (Mixtures 1 and 2; Table 2) were used to collect the data for estimating model parameters. Under the feed conditions listed in Mixture 1, the catalyst was never exposed to any reductant and therefore, the obtained experimental data can be used to estimate the kinetic parameters for reactions (1)–(6) (Table 1) independent of reactions (7)–(11) (Table 1). Accordingly, in the first phase of the parameter estimation, the reduced model with only the first 6 reactions was studied. The rate constant for the NO oxidation reaction, k_1, was tuned to obtain the conversion equal to the value observed when the catalyst reaches its saturation limit in terms of storing the NO_x. In Fig. 5, this corresponds to a time greater than 2500 s. The equilibrium constant, K_1^{eq}, was obtained from thermodynamic calculations whereas the constant in the inhibition term, K_1, was taken from the literature [9]. The remaining model parameters ($k_2, \ldots, k_5, D_{eff}, X_1, Y_1, X_2, Y_2$) were estimated after an extensive trial and error exercise to minimize the sum of square errors between the predicted and measured exit NO_x concentration profiles over 15 cycles, starting from the fresh/clean catalyst.

During the first lean phase of cyclic operation, the radial position defining the reaction front within the catalyst particle was calculated using the following expression:

$$r_f = r_{tot} * \left(\frac{0.5 * \theta_{BaCO_3}}{1 - 0.5 * \theta_{BaCO_3}}\right)^{1/3} \quad (16)$$

However, during the following rich phase, the amount of CO_2 may be enough to reach all the nitrate species in the proposed particle and therefore, as discussed in the previous section, all of them may get converted back into the freshly available storage sites via

Table 2
Feed compositions during lean and rich phases.

Gas species	Mixture 1		Mixture 2		Mixture 3	
	Lean phase	Rich phase	Lean phase	Rich phase	Lean phase	Rich phase
NO	330 ppm	0 ppm	330 ppm	0 ppm	330 ppm	0 ppm
O_2	10%	0%	10%	0%	10%	0%
CO_2	5%	5%	5%	5%	5%	5%
H_2O	5%	5%	5%	5%	5%	5%
CO	0%	0%	0%	1.5%	0%	3%
N_2	Balance	Balance	Balance	Balance	Balance	Balance

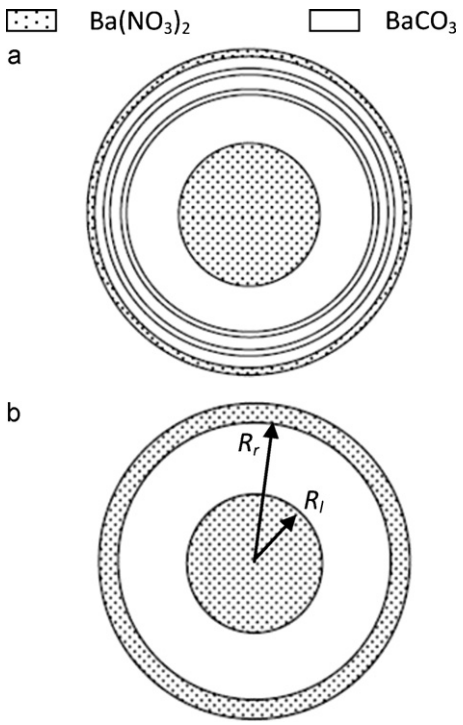

Fig. 4. Configuration of the storage particle after rich phase (a) considering the regeneration of multiple types of storage sites and (b) confining all regenerated storage particles to a single layer.

self-decomposition reactions (cf. reactions (4) and (5); Table 1). In case of incomplete regeneration, this may result in the formation of multiple rings within the nitrate layer representing different types of storage sites regenerated. The resulting particle configuration is schematically illustrated in Fig. 4a. The NO_x released due to the self-decomposition reactions will, therefore, be available in the vicinity of these different storage sites, and this will result in the occurrence of multiple storage reactions simultaneously. However, as a simplification, their average effect was considered using an average radial position. During the subsequent lean phases, the NO_x in the feed has to react with the multiple storage sites, formed during the rich phase, before reacting with the inner carbonate core (see Fig. 4a). In order to simplify the computation of the reaction front within these multiple radial positions, the multiple rings of storage sites were first assumed to be confined to a single layer starting from the catalyst surface as shown in Fig. 4b. The radial position of the carbonate–nitrate interface within this uppermost layer can then be calculated using following expression:

$$r_f'' = r_{tot} * \left(\frac{0.5 * \theta_{BaCO_3} - (1 - 0.5 * \theta_{BaCO_3}) * (R_l/r_{tot})^3 + (1 - 0.5 * \theta_{BaCO_3}) * (R_r/r_{tot})^3}{1 - 0.5 * \theta_{BaCO_3}} \right)^{1/3} \quad (17)$$

Here, R_l and R_r are the radial positions for the carbonate–nitrate interfaces, obtained at the end of the last lean phase and rich phase, respectively.

To account for the existence of multiple carbonate rings, the radius of the carbonate–nitrate interface, calculated from the above equation, needs to be distributed along the whole nitrate layer. This was achieved by multiplying the calculated radius value by a sigmoid function which depends on the difference between carbonate fraction during the present and previous lean phases. The expression for the modified radius position is given as follows:

$$r_f = (r_f'' - R_l) * fls2hs(\theta_{BaCO_3} - \theta'_{BaCO_3} + a, b) + R_l \quad (18)$$

Here, θ'_{BaCO_3} is the carbonate fraction obtained at the end of the last lean phase and "*flc2hs*" is the COMSOL function used to represent the sigmoid function, controlled by the parameters "*a*" and "*b*".

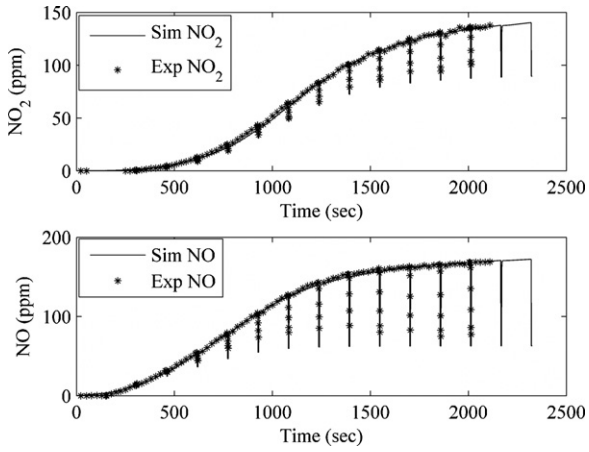

Fig. 5. The simulated and experimental NO and NO_2 concentration profiles at the catalyst exit during the cyclic operation. Started with a completely regenerated catalyst under the inlet feed composition, listed as Mixture 1 (c.f. Table 2).

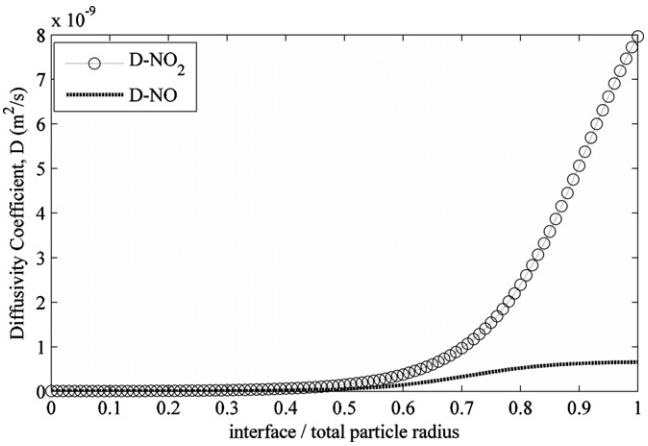

Fig. 6. The estimated diffusivity coefficient as a function of the ratio of interface position to total particle radius.

After consuming the uppermost carbonate layer, the particle's configuration resembles the one obtained during the previous lean phase and accordingly, the radial position for the reaction front can now be calculated using Eq. (16). The model predictions and corresponding experimental data are presented in Fig. 5, which shows an excellent agreement between the two. Fig. 6 shows a plot of the estimated diffusivity coefficient, $D(r)$, as a function of radial position within the particle as per Eq. (15). As can be seen, the function is highly nonlinear, spanning a very large range of values over the entire depth of the proposed particle, which strongly indicates the presence of multiple storage site types with a very wide range of reaction rates. Further evidence in support of this conclusion was drawn from a simulation study, where the diffusivity coefficient in the storage reactions was set constant. The assumption of a constant diffusivity coefficient neglects the effects of different storage reaction rates and only considers pore diffusion through the nitrate layer as proposed in the work by Olsson et al. [1]. This assumption could be based on two possibilities; either there is only a single type of storage site present in the catalyst or if there are different storage sites, they all result in similar reaction rates. In one of the simula-

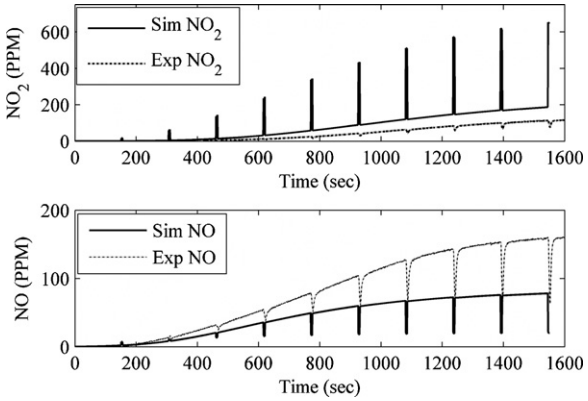

Fig. 7. The simulated and experimental NO and NO_2 concentration profiles at the catalyst exit during the cyclic operation. Started with a completely regenerated catalyst under the inlet feed composition, listed as Mixture 1 (c.f. Table 2). The model was solved under the assumption of constant diffusivity coefficient.

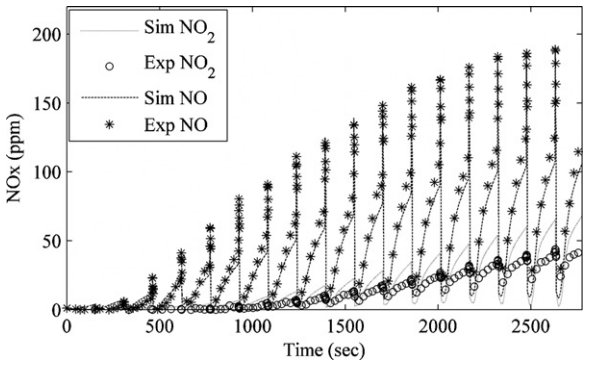

Fig. 8. The simulated and experimental NO and NO_2 concentration profiles at the catalyst exit during the cyclic operation. Started with a completely regenerated catalyst under the inlet feed composition, listed as Mixture 2 (c.f. Table 2).

tion studies considering a constant diffusivity coefficient, a single type of storage particle was assumed using $BaCO_3$ as the proposed particle. The rates of the backward reactions were obtained from thermodynamic calculations between carbonate and nitrate, in a way similar to the one reported by Olsson et al. [1]. The simulated exit NO_x concentration profile is compared with the experimental data in Fig. 7 and as can be seen, a single type of storage particle resulted in over-prediction in the NO_2 concentration during the rich phase. As two of the gas species, O_2 and NO, were not in the feed during the rich phase, the backward or self-decomposition reactions dominate the storage reactions and therefore, it is obvious that in order to lower the NO_2 concentrations in the rich phase, the rate constants for the backward or self-decomposition reactions should be lower than the ones calculated using the thermodynamic equilibrium between carbonate and nitrate. This indicates that in addition to the carbonates, the storage sites may also be present in other forms, such as oxides and hydroxides, because their co-existence may affect the overall equilibrium constant between storage and self-decomposition reactions. Moreover, lowering the self-decomposition reaction rates will also lower the predicted NO and NO_2 concentrations during the lean phase, and to reverse this decrease, the rates of the corresponding storage reactions have to be decreased over a period of time as storage proceeds. This progressive decrease in the rates of storage reactions was accounted for in this work using a varying diffusivity coefficient.

In the second phase of the parameter estimation, reductant based reactions (cf. reactions (7)–(11); Table 1) were also added to the model. This final model includes the estimated parameters from the discussion above and also the unknown kinetic parameters associated with only reductant-based reactions. Using experimental data obtained under the feed conditions listed for Mixture 2 (Table 2), a trial and error procedure was implemented to search the best possible estimates for the unknown kinetic parameters minimizing the sum of square errors between the predicted and measured exit NO_x concentration profiles over the first 20 cycles. The radial position of the carbonate–nitrate interface during the first lean phase was calculated using Eq. (16). During the rich phase, the amount of reductant may or may not be sufficient to reach all the nitrate particles. However, there is a possibility that the Pt/Ba proximity may affect the regeneration reactions to a certain extent and therefore, as an initial approximation, it was considered that the nitrates at the particle surface (close to the Pt sites) will react first, followed by the nitrates within subsequent inner layers. In the case of incomplete regeneration at the end of the rich phase, this will result in a particle with two carbonate layers, as shown earlier in Fig. 4b. Therefore, during the subsequent lean phases, the radial position of the carbonate–nitrate interface was calculated first using Eq. (17), when the uppermost carbonate layer was being consumed, and then using Eq. (16), when the innermost carbonate core was being consumed, as discussed above.

After extensive simulation trials, the best possible predictions obtained for the NO and NO_2 concentration profiles are shown in Fig. 8. As can be seen, the agreement between predicted and experimental NO and NO_2 concentration profiles decreases with each cycle. In order to improve the model predictions, there are two possibilities that were investigated. The first was increasing the rate of the NO_2 storage reaction, which will lower the predicted NO_2 concentration. But with this modification, the NO concentration will also decrease and therefore, the deviation between predicted and experimental NO concentration profile will increase further. To counter this deviation, the rate of the NO storage reaction has to be decreased at the same time. The second possibility is to decrease the NO oxidation rate which will lower the NO_2 formation thus decreasing the NO_2 concentration and simultaneously increasing the NO concentration as required. A possible reason for these modifications in the reaction rates may be that after getting exposed to the reductants, the catalyst structure may have changed, due to which the catalyst now favors NO_2 storage more than that of NO, relative to the one already predicted during the cyclic operation without reductants, or now has relatively less oxidation capability. At this point, there is no experimental evidence to support the hypothesis that the CO might have changed the storage rates and therefore the modifications in the diffusivity function based on this hypothesis were not implemented in this study. On the other hand, the effect of CO on the Pt sites has been well studied in the past [13,17,18]. First, the exposure of the catalyst to CO could lead to residual CO poisoning of the Pt sites which may deteriorate catalytic NO oxidation during the subsequent lean phase [13]. Second, with CO as the reductant source, isocyanates form around the Pt sites [18,19] which may affect their oxidation ability.

A decrease in the rate of NO oxidation resulted in a significant improvement as shown in Fig. 9. It should be noted that during the transient cyclic regime, the NO oxidation rate was lowered progressively after every rich phase until the steady state regime is obtained where, it is 35% of the value, estimated from the cyclic experiment with no reductant (cf. Mixture 1; Table 2). Moreover, this decrease was limited only to the region which had been exposed to CO and everywhere else in the reactor, the oxidation rate was kept at the value previously estimated for start-up cyclic operation with no reductant. A reduction in the NO oxidation reaction rate has also been proposed in a recent study by Schmeißer et al. [20] to explain their model predictions.

Fig. 10 shows the predicted carbonate fraction along the catalyst length at the end of different lean and rich phases. It is clear

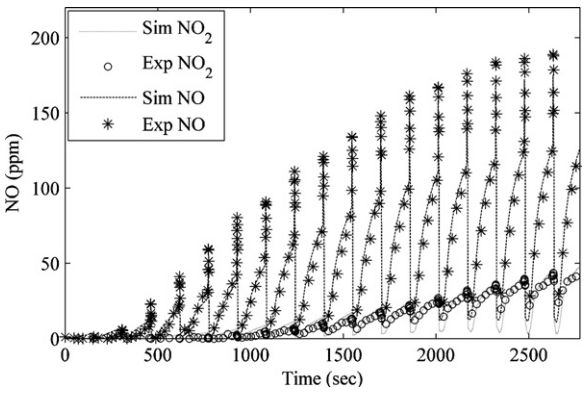

Fig. 9. The simulated and experimental NO and NO_2 concentration profiles at the catalyst exit during the cyclic operation. Started with a completely regenerated catalyst under the inlet feed composition, listed as Mixture 2 (c.f. Table 2) and reduced NO oxidation rate in the catalyst region which have been exposed to the reductants during the previous rich phase.

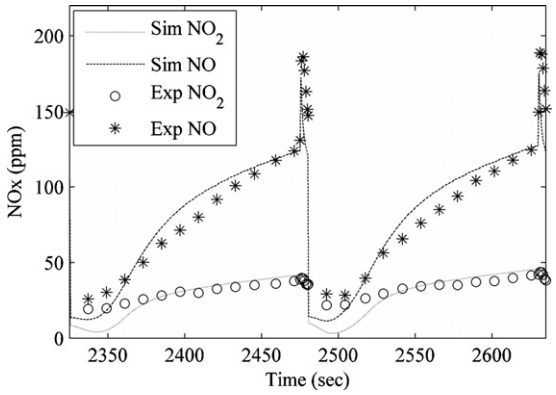

Fig. 11. The simulated and experimental NO and NO_2 concentration profiles at the catalyst exit over two consecutive cycles in the steady cyclic regime the cyclic operation. Started with a completely regenerated catalyst under the inlet feed composition, listed as Mixture 2 (c.f. Table 2) and reduced NO oxidation rate in the catalyst region which have been exposed to the reductants during the previous rich phase.

that only a fraction of the upstream portion of the catalyst is being significantly regenerated, and the extent of regeneration decreases until the point at which the reductant is completely consumed. The downstream portion of the catalyst beyond this point is initially involved only in the storage reactions. Eventually, after a certain number of cycles, this portion of the catalyst will reach its saturation limit for storing NO_x and from then on, only the amount of catalyst being regenerated during the rich phase will be used. This corresponds to the period when the catalyst operation is in the steady cyclic regime. An estimate of the storage sites that can be regenerated during the rich phase, based on stoichiometric calculations, also agrees with the model prediction. During the lean phase, the catalyst is exposed to approximately 0.25 mmol of NO_x and this amount will consume 0.13 mmol of the storage sites based on stoichiometric analysis. During the rich phase, in the period of 5 s with 1.5% CO, 0.38 mmol of reductant are added to the catalyst. Based on the reaction stoichiometry, 0.3 mmol of reductant will react in regeneration reactions (cf. reactions (9) and (10); Table 1) which are just sufficient to regenerate only 0.076 mmol of the storage sites. Therefore in one cycle, the percentage of storage sites being regenerated is ~61%, which is approximately similar to that predicted in the model results shown in Fig. 10.

Fig. 11 compares the predicted and experimental NO and NO_2 concentration profiles over two consecutive cycles in the steady cycle-to-cycle regime. During the initial period of the lean phase, the model predicts relatively high storage rates, resulting in lower NO and NO_2 concentrations as compared to the experiments. The maximum difference in the exit NO_x concentration is about 15% of the inlet concentration. A plausible explanation for this discrepancy comes from the assumption of nitrates being close to the surface reacting first before the nitrate in subsequent inner layers. In reality, the Pt/Ba proximity effect on the regeneration reactions may not be as severe as assumed and therefore, 1.5% CO may be sufficient to reach all the nitrates at the same time. In the case of incomplete regeneration, this may lead to the formation of multiple layers of storage sites within the nitrate layer formed during the previous lean phase and the particle configuration may resemble the one proposed earlier in Fig. 4a. In that case, for the subsequent lean phase, the amount of carbonate distributed over a certain depth inside the nitrate layer as per Fig. 4a would give lower storage rates as compared to the same amount of carbonate when assumed to be confined to the surface (as in Fig. 4b). However, additional experimental knowledge on the distribution of the carbonates is required and therefore, inclusion of this effect into the model is left for future work.

To verify the validity of the model, an additional operating scenario (Mixture 3; Table 2) was used. Starting with a fresh catalyst condition, the model was first simulated under the feed conditions specified in Mixture 2 (Table 2) until steady cycle-to-cycle operation was obtained and then under the feed conditions specified in Mixture 3 (Table 2), again until steady cycle-to-cycle operation was obtained. Fig. 12 compares the predicted and experimental NO and NO_2 concentration profiles over two consecutive cycles

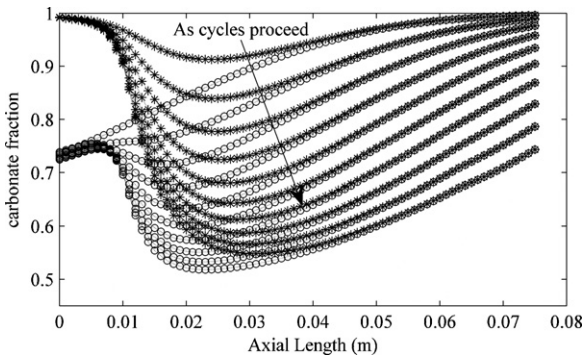

Fig. 10. The predicted carbonate fraction along the catalyst length at the end of lean phase (stars) and rich phase (circles). The fraction keeps on decreasing with the increase in cycles.

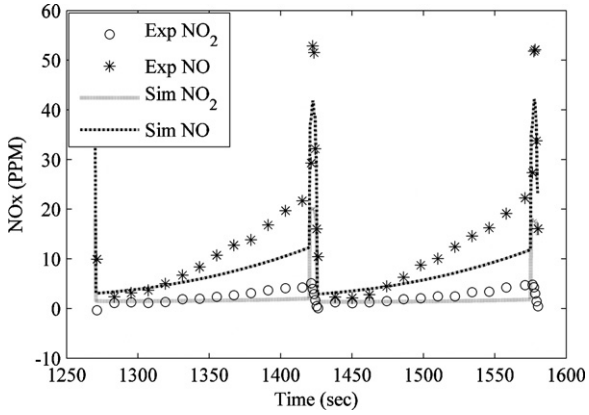

Fig. 12. The simulated and experimental NO and NO_2 concentration profiles at the catalyst exit over two consecutive cycles once the steady cyclic regime is obtained under the inlet feed composition, listed as Mixture 3 (c.f. Table 2).

in the steady cycle-to-cycle regime corresponding to the feed composition of Mixture 3. As can be seen, the predicted NO and NO_2 concentrations in the lean phase are slightly lower than the experimental data. The maximum difference in the overall NO_x concentration is about 6% of the inlet concentration. The slight discrepancies between data and model predictions can be attributed to the assumption of nitrates being close to the surface reacting first before the nitrate in subsequent inner layers as discussed for the previous case.

4. Conclusions

A 1D mathematical model of a commercial NSR catalyst has been proposed. To account for the existence of storage particles with different storage capacities, an idealized representation of a storage particle is proposed in which a diffusivity coefficient that controls the diffusion of NO_x species within the particle decreases as a nonlinear function of the particle depth. As a result, the diffusion resistance within the particle represents the different storage rates as the NO_x penetrates into the particle. The proposed approach is generic in the sense that the varying diffusivity coefficient function can account for any number of different types of storage sites without any quantitative information. In this paper, it is also assumed that during the regeneration process, the storage sites with the highest rates are regenerated first followed by the sites with relatively lower rates. From the simulation results obtained for start-up operation (cf. Mixture 2), very high storage is predicted during the very initial period of the lean phases indicating that the storage sites, regenerated during incomplete regeneration in the rich phase, may be distributed more uniformly across the nitrate layer rather than being concentrated at the outer layer of the catalyst particles, thus lowering the average storage capacity. Moreover, in order to obtain a reasonable agreement between the predictions and the experimental data for NO_x, the NO oxidation reaction rate had to be reduced in the catalyst region which has been exposed to the reductant during the previous regeneration phase. On overall, the model is able to explain the experimental NO_x concentration profiles in both transient and steady cycle-to-cycle regimes, and therefore has the potential to be used for optimization and control purposes for real-life driving scenarios.

Acknowledgements

The authors would like to acknowledge Natural Science and Engineering Research Council (NSERC) for financial support and Johnson Matthey for providing the commercial catalyst used to collect the experimental data for this work.

References

[1] L. Olsson, R.J. Blint, E. Fridell, Global kinetic model for lean NO_x traps, Ind. Eng. Chem. Res. 44 (2005) 3021–3032.
[2] L. Olsson, D. Monroe, R.J. Blint, Global kinetic modelling of a supplier barium and potassium containing lean NO_x trap, Ind. Eng. Chem. Res. 45 (2006) 8883–8890.
[3] P. Kočí, M. Marek, M. Kubíček, T. Maunula, M. Härkönen, Modelling of catalytic monolith converters with low and high temperature NO_x storage compounds and differentiated washcoat, Chem. Eng. J. 97 (2004) 131–139.
[4] P. Kočí, M. Schejbal, J. Trdlička, T. Gregor, M. Kubíček, M. Marek, Transient behaviour of catalytic monolith with NO_x storage capacity, Catal. Today 119 (2007) 64–72.
[5] A. Güthenke, D. Chatterjee, M. Weibel, N. Waldbüßer, P. Kočí, M. Marek, M. Kubíček, Development and application of a model for a NO_x storage and reduction catalyst, Chem. Eng. Sci. 62 (2007) 5357–5363.
[6] V. Schmeißer, U. Tuttlies, G. Eigenberger, Towards a realistic simulation model for NO_x-storage catalyst dynamics, Top. Catal. 42–43 (2007) 77–81.
[7] U. Tuttlies, V. Schmeißer, G. Eigenberger, A mechanistic simulation model for NO_x storage catalyst dynamics, Chem. Eng. Sci. 59 (2004) 4731–4738.
[8] B.R. Kromer, L. Cao, L. Cumaranatunge, S.S. Mulla, J.L. Ratts, A. Yezerets, N.W. Currier, F.H. Ribeiro, W.N. Delgass, J.M. Caruthers, Modeling of NO oxidation and NO_x storage on $Pt/BaO/Al_2O_3$ NO_x traps, Catal. Today 136 (2008) 93–103.
[9] J. Jirát, M. Kubíček, M. Marek, Mathematical modelling of catalytic monolithic reactors with storage of reaction components on the catalyst surface, Catal. Today 53 (1999) 583–596.
[10] S. Kojima, N. Baba, S. Matsunaga, K. Senda, K. Katoh, T. Itoh, Modeling and Numerical Analysis of NO_x Storage-Reduction Catalysts—On the Two Effects of Rich-Spike Duration, SAE Technical Paper, 2001-01-1297.
[11] J.S. Hepburn, E. Thanasiu, D.A. Dobson, W.L. Watkins, Experimental and Modeling Investigations of NO_x Trap Performance, SAE Technical Paper, 962051.
[12] J.S. Hepburn, T.E. Kenney, J. McKenzie, E. Thanasiu, M.A. Dearth, Engine and Aftertreatment Modeling for Gasoline Direct Injection, SAE Technical Paper, 982596.
[13] M. Al-Harbi, W.S. Epling, The effects of regeneration-phase CO and/or H_2 amount on the performance of a NO_x storage/reduction catalyst, Appl. Catal. B 89 (2009) 315–325.
[14] M. Al-Harbi, W.S. Epling, A. Yezerets, N.W. Currier, H.Y. Chen, H. Hess, The Effects of Thermal Degradation on the Performance of a NOx Storage/Reduction Catalyst, SAE Technical Paper, 2009-01-0631.
[15] S.S. Mulla, N. Chen, W.N. Delgass, W.S. Epling, F.H. Ribeiro, NO_2 inhibits the catalytic reaction of NO and O_2 over Pt, Catal. Lett. 100 (2005) 267–270.
[16] W.S. Epling, L.E. Campbell, A. Yezerets, N.W. Currier, J.E. Parks II, Overview of the fundamental reactions and degradation mechanisms of NO_x storage/reduction catalysts, Catal. Rev. 46 (2004) 163–245.
[17] S.E. Voltz, C.R. Morgan, D. Liederman, S.M. Jacob, Kinetic study of carbon monoxide and propylene oxidation on platinum catalysts, Ind. Eng. Chem. Prod. Res. Dev. 12 (1973) 294–301.
[18] T. Lesage, C. Verrier, P. Bazin, J. Saussey, M. Daturi, Studying the NO_x-trap mechanism over a $Pt–Rh/Ba/Al_2O_3$ catalyst by operando FT-IR spectroscopy, Phys. Chem. Chem. Phys. 5 (2003) 4435–4440.
[19] T. Szailer, J.H. Kwak, D.H. Kim, J.C. Hanson, C.H.F. Peden, J. Szanyi, Reduction of stored NO_x on Pt/Al_2O_3 and $Pt/BaO/Al_2O_3$ catalysts with H_2 and CO, J. Catal. 239 (2006) 51–64.
[20] V. Schmeißer, G. Eigenberger, U. Nieken, An improved model for NO_x-storage catalysts, Top. Catal. 52 (2009) 1934–1939.